# The origin of discontinuous yielding in Mg alloys under slip-dominated condition studied by in-situ synchrotron diffraction and elastic-viscoplastic self-consistent modeling

Y.Q. Chi[a], X.H. Zhou[b], C. Xu[a], D. Sun[a], X.G. Qiao[a], H.G. Brokmeier[b,c], M.Y. Zheng[a,*]

[a] School of Materials Science and Engineering, Harbin Institute of Technology, Harbin, 150001, PR China

[b] Institute of Materials Science and Engineering, Clausthal University of Technology, Agricolastrasse 6, D-38678, Clausthal-Zellerfeld, Germany

[c] Helmholtz Zentrum Geesthacht, Max Planck Straße 1, D-21502, Geesthacht, Germany

## Abstract

A discontinuous yielding was observed in the as-extruded Mg-7Gd-2Y-1Zn-0.6Zr (wt. %) alloy under uniaxial tension along the extrusion direction, which was eliminated by the peak-aging treatment. The deformation mechanisms of the as-extruded and peak-aged alloys were studied by in-situ synchrotron diffraction measurement and elastic-viscoplastic self-consistent (EVPSC) modeling. The in-situ synchrotron diffraction results suggest that the unpinning of basal dislocations from solute atmospheres causes the stress relaxation in the basal slip favored grains. The EVPSC modeling results indicate that the discontinuous yielding in the as-extruded alloy is associated with the interaction between basal dislocations and solute atmospheres. After peak-aging treatment, the interaction between basal dislocations and solute atmospheres is weakened

due to the consumption of a number of solute atoms. Consequently, the discontinuous yielding is eliminated in the peak-aged alloy.

**Keywords:** magnesium alloys, discontinuous yielding, synchrotron diffraction, elastic-viscoplastic self-consistent, stress relaxation

## 1. Introduction

The plasticity of Mg alloys involves several deformation modes, including basal slip, non-basal slip and deformation twinning [1], among which basal slip is the softest one. Consequently, basal slip is always firstly activated, contributing to the micro yielding [2-3]. It was pointed out that non-basal slip or twinning dominates the macro yielding of wrought Mg alloys which possess strong texture [2-5]. Even in the randomly textured Mg alloys, these hard deformation mechanisms are still required to permit macro yielding [6]. Under twinning-dominated conditions, a low work hardening stage, including a possible Lüders plateau, appears upon the initiation of macro yielding, followed by a high hardening region [7-8]. The appearance of the low hardening region is suggested due to the collaborative nucleation of twinning [4]. Contrarily, in the slip-dominated cases, the strain hardening rate is always continuously decreased during the elastoplastic transition stage [7]. An exception exists when the yield point occurs, which commonly involves a yield stress drop and a yield plateau, giving rise to the discontinuous yielding behavior. This phenomenon has been observed in many Mg alloys

produced by various processing methods, such as as-extruded Mg-Zn-Zr-Er alloys [9], rolled and annealed Mg-Gd alloys [10], as-extruded Mg-Nd(-Zn)-Zr alloys [11], as-extruded Mg-Zn-Y alloys [12] et al. Within these studies, the occurrence of yield point was simply attributed to the interaction between dislocations and solute atmospheres or precipitates, as firstly proposed by Cottrell and Bilby [13], while the detailed investigations, e.g. the specific dislocation type contributing to this phenomenon and its effect on the deformation behavior, were lacked.

In this work, we observed a discontinuous yielding under uniaxial tension along the extrusion direction (ED) of the as-extruded Mg-7Gd-2Y-1Zn-0.6Zr (wt. %) alloy, which disappeared after peak-aging treatment. To examine the underlying mechanisms governing this yielding behavior, the in-situ synchrotron diffraction testing and elastic-viscoplastic self-consistent (EVPSC) modeling were applied to the as-extruded and peak-aged alloys. The in-situ synchrotron diffraction measurement can provide grain-level information for variously oriented grain sets (a collection of grains with similar orientation), including the lattice strain and diffraction intensity evolutions during loading process, which is especially useful to study the plastic deformation behavior of Mg alloys which possess nearly elastic isotropy and plastic anisotropy. Polycrystal plasticity modeling has been widely applied to interpret the in-situ diffraction results and draw quantitative findings, such as the activation stress of individual slip/twinning systems [6] and the operation of deformation mechanisms [3].

## 2. Experimental procedures

The Mg-7Gd-2Y-1Zn-0.6Zr (wt. %) alloy was fabricated by direct-chill (DC) casting. Billets with diameter of 42 mm and height of 35 mm were cut from the cast ingots. After homogenization at 510$^{o}$C for 8h and water quenching, the billets were subjected to indirect extrusion, conducted at 400$^{o}$C with a ram speed of 0.1 mm/s and an extrusion ratio of 12. The homogenized billet was not placed in the extrusion container until the container temperature reached 400℃. Afterwards, the billet was heated in the container for 15min to homogenize the sample temperature before the extrusion force was imposed. After the completion of extrusion, the extruded bar was immediately subjected to water quenching. Finally, round bars with dimensions of Φ 12.5 × 270 mm were obtained. Some extruded bars were further peak-aged at 200$^{o}$C for 84h. The microstructure was observed by ZEISS Supra 55 SAPPHIRE scanning electron microscope (SEM) equipped with an electron backscattered diffraction (EBSD) detector and Talos F200X Transmission electron microscope (TEM) operating at 200kV. The step size during EBSD measurement is 0.3 μm for both alloys.

The synchrotron diffraction measurement was performed under in-situ uniaxial tension at the P07-HEMS beamline of PETRA III, at the DeutschesElektronen-Synchrotron (DESY). Tensile bars with 4 mm in diameter and 24 mm in gauge length were cut from the extruded bars with the loading axis along ED. The tensile loading was applied continuously under

displacement control at room temperature with a displacement rate of 0.001 mm/s. The diffraction patterns as a function of 2θ were obtained by azimuthal integrating the Debye-Scherrer rings between ± 5$^{o}$ about the loading axis, using the software of Fit2D. Afterwards, the diffraction patterns were analyzed by a single-peak fitting approach to determine the peak positions, following which the lattice spacing can be obtained by applying the Bragg diffraction relationship. Subsequently, the lattice strains within grains that satisfy the Bragg condition for a given (hkl) reflection were computed following the equation:

$$\varepsilon^{hkl} = \frac{d^{hkl} - d_0^{hkl}}{d_0^{hkl}} \quad (1)$$

where $d^{hkl}$ is the measured lattice spacing, and $d_0^{hkl}$ is the lattice spacing prior to mechanical loading.

The EVPSC model, which was originally developed during 1980's by Molinari et al. [14], was recently implemented by Wang et al. [15], in a way which is applicable to large strain and to arbitrary crystal structure. It is generally assumed that the plastic deformation of a crystal is attributed to slip and twinning modes. In this work, three slip modes and one twinning mode are considered, including {00.2} <11.0> basal slip, {10.0} <11.0> prismatic slip, {11.2} <11.3> pyramidal <c+a> slip and {10.2} <10.1> extension twinning. At the grain level, the plastic strain rate $\dot{\varepsilon}_p$ is calculated by the following equation:

$$\dot{\varepsilon}_p = \sum_\alpha \dot{\gamma}^\alpha \boldsymbol{P}^\alpha \quad (2)$$

where $\dot{\gamma}^{\alpha}$ and $\boldsymbol{P}^{\alpha}$ are shear rate and Schmid tensor of slip/twinning system α, respectively.

Following Asaro and Needleman [16], the shear rate of slip/twinning system can be described by the power law.

For slip system α:

$$\dot{\gamma}^{\alpha} = \dot{\gamma}_0 |\tau^{\alpha}/\tau_{cr}^{\alpha}|^{\frac{1}{m}} sgn(\tau^{\alpha}) \tag{3}$$

For twinning system α, considering the polar nature of twinning, the relation is:

$$\dot{\gamma}^{\alpha} = \begin{cases} \dot{\gamma}_0 |\tau^{\alpha}/\tau_{cr}^{\alpha}|^{\frac{1}{m}} & \tau^{\alpha} > 0 \\ 0 & \tau^{\alpha} < 0 \end{cases} \tag{4}$$

where $\dot{\gamma}_0$ is the reference shear rate, $\tau^{\alpha}$ is the resolved shear stress, $\tau_{cr}^{\alpha}$ is the critical resolved shear stress (CRSS) and m is the strain rate sensitivity.

An empirical extended Voce hardening rule is incorporated into the EVPSC model to account for the evolution of CRSS $\tau_{cr}^{\alpha}$ for both slip and twinning, as following.

$$\dot{\tau}_{cr}^{\alpha} = \frac{d\hat{\tau}^{\alpha}}{d\Gamma} \sum_{\beta} h^{\alpha\beta} \left|\dot{\gamma}^{\beta}\right| \tag{5}$$

where $\Gamma = \sum_{\alpha} \int |\dot{\gamma}^{\alpha}| dt$ is the accumulated shear strain in the grain, and $h^{\alpha\beta}$ is the latent hardening coupling coefficient which empirically determines the obstacles of system β on system α. For simplicity, all $h^{\alpha\beta}$ in the present modeling are equal to 1, assuming that every slip and twinning system hardens itself and all other systems equally. The threshold stress $\hat{\tau}^{\alpha}$ is determined by:

$$\hat{\tau}^{\alpha} = \tau_0^{\alpha} + (\tau_1^{\alpha} + \theta_1^{\alpha}\Gamma)(1 - \exp(-\frac{\theta_0^{\alpha}\Gamma}{\tau_1^{\alpha}})) \tag{6}$$

Here, $\tau_0^\alpha$ is the initial CRSS, $\theta_0^\alpha$ and $\theta_1^\alpha$ correspond to the initial and terminal strain hardening rates, and $\tau_1^\alpha$ is the back-extrapolated flow stress.

The EVPSC modeling was conducted with employing a linearization scheme of $n_{eff}$ =10. The polycrystal is approximated by 10000 discrete orientations, whose volume fractions are weighted in order to mimic the initial textures of the alloys. The tensile loading was imposed with a strain rate of $0.0001s^{-1}$, and the reference slip/twinning rate applied the same value to the loading strain rate. The strain rate sensitivity is 0.05, which is prescribed to be the same for all the slip and twining systems.

## 3. Results and discussions

Fig. 1 shows the EBSD results of the alloys. The as-extruded alloy exhibits a bi-modal microstructure, consisted of fine dynamically recrystallized (DRXed) grains with a mean diameter of 1.4 μm and elongated non-dynamically recrystallized (non-DRXed) grains. The fraction of DRXed regions is about 26.8%. The non-DRXed grains exhibit strong fiber texture with <10.0> axis parallel to ED, while the DRXed grains have very weak texture. The bi-modal microstructure is retained after peak-aging treatment, and the peak-aged alloy has similar recrystallization fraction (27.7%) and DRXed grain size (1.39 μm) to the as-extruded alloy, indicating no significant recrystallization or grain growth occur during the peak-aging treatment. Additionally, the texture of the DRXed and non-DRXed regions is nearly unaffected by the

peak-aging treatment. The large black areas in Fig. 1c indicate blocky long-period stacking ordered (LPSO) phases, which are not indexed. In fact, the as-extruded alloy also contains LPSO phases (results are not shown here). The fraction of blocky LPSO phases in both alloys is about 3%, and peak-aging treatment does not affect this phase.

Fig. 2 shows the TEM micrographs of the alloys. In the as-extruded alloy, some particles are observed in the DRXed regions, as indicated by the arrows in Fig. 2a. These particles are identified to be β-$Mg_5RE$ phases [ 17 - 18 ], commonly observed in Mg-Gd alloys after thermomechanical processing. Lamellar phases are found within some DRXed and non-DRXed grains, as indicated by the triangles in Fig.2a and b. According to the selected area electron diffraction (SAED) pattern, they are γ' phases formed during extrusion. The peak-aging treatment does not notably affect the β or γ' phases, while it leads to the precipitation of substantial β' phases, as illustrated in Fig. 2e and f.

Fig. 3 presents the tensile flow curves of the alloys, along with the strain hardening rate normalized by the shear modules of Mg (G= 17.6 GPa) as a function of true strain. After peak-aging treatment, the tensile yield strength is enhanced from 360 MPa to 400 MPa, whereas the elongation to failure is decreased by 5%. The peak-aged alloy exhibits a typical elastoplastic transition dominated by dislocation slip [7], namely, the strain hardening rate continuously decreases after the plasticity is activated. However, the as-extruded alloy exhibits a

discontinuous yielding behavior, specifically, the hardening rate abruptly drops to 0.07 G when the plasticity is initiated, followed by a slight increase to 0.1 G, after which the hardening rate slowly decreases.

Fig. 4 shows the flow curves, lattice strains and diffraction intensities of the alloys plotted against the applied macro stress. The flow curves are included to facilitate the comparison of overall sample response and individual grain set performance. It is noteworthy that the lattice strains shown here provide information about variously oriented grains that present their {hk.l} poles parallel to the loading direction (referred to as "{hk.l} grains" hereinafter). Due to the nearly elastic isotropy of Mg alloys, all grain sets undergo straining quite similarly at the elastic stage. However, once the plastic deformation occurs in a given grain set, the grains of this set will not load as much stress as they do at the elastic stage. In the meantime, the other grain sets with harder orientations need to share more load. As a consequence, the lattice strain curves of the related grain sets will deviate from the elastic linearity, with softer and harder oriented grains accumulating their lattice strains slower and faster than that at the elastic stage, respectively.

As shown in Fig. 4b, the as-extruded alloy undergoes elastic deformation until about 360 MPa (macro yielding), at which stress the {10.1} grains exhibit abrupt relaxation, i.e. the lattice strain suddenly decreases while the loading stress is only slightly raised. Since the {10.1} grains are favorable for basal slip [6], the relaxation is mainly associated with the activation of this slip

mode. Before straining again, the lattice strain decrement in the {10.1} grains is approximately 2736 με, indicating the stress relaxation by 123 MPa. Meanwhile, the lattice strains in other grain sets, including the {10.0}, {11.0} and {00.2} grains, are increased with a larger rate than at the elastic stage after macro yielding, suggesting these grains are bearing more load. With further loading to 365MPa, the {11.0} grains show slight relaxation. The lattice strain curve of {10.0} grains displays an inflection at about 373 MPa, after which the grains accumulate strain slightly slower than at the previous stage. For the {11.0} and {10.0} grains, the plastic deformation under tensile loading is preferentially accommodated by prismatic slip, owing to the inhibition of basal slip and tensile twinning in these grains. So, the relaxation of {11.0} grains and the inflection in the lattice strain curve of {10.0} grains correspond to the operation of prismatic slip [6]. Finally, the lattice strain in {00.2} grains shows an abrupt negative jump at 381 MPa. These grains are ideally oriented for tensile twinning when they are imposed tensile loading along c-axis, and the twinning involves stress relaxation [19].

As shown in Fig. 4c, the {10.0} grains in the as-extruded alloy have the highest diffraction intensity, followed by the {10.1} grains, whereas both {11.0} and {00.2} grains possess very low intensity. These results are in well agreement with the EBSD observations shown in Fig. 1. Specifically, the {10.0} grains mainly originate from the non-DRXed regions with a large fraction, thus giving rise to the strong intensity. The other grain sets are primarily

attributed to the DRXed regions, which are nearly randomly oriented. During the elastic stage, the intensities of all grain sets are unchanged, since no crystal reorientation happens. However, upon the occurrence of relaxation in the {10.1} and {11.0} grains, their intensities exhibit abrupt drop, which is due to the operation of basal and prismatic slip, respectively. The intensity decrease of {00.2} grains is due to the tensile twinning, since the twinned regions reorient their crystal about {11.0} axis by ~86°. However, it should be pointed out that the intensity of {00.2} grains is rather low, so the tensile twinning only contributes slightly to the deformation.

In the peak-aged alloy, the lattice strain curve of {10.1} grains starts to deviate from the linear elasticity when loaded to 334 MPa, which is lower than the macro yielding stress (Fig. 4e). Specifically, these grains tend to accumulate strain with a much lower rate than at the elastic stage until 374 MPa, after which an obvious relaxation occurs, reducing the lattice strain by 1754 με. Note that this decrement is much smaller than that of the as-extruded alloy (2736 με). Meanwhile, the other grain sets possess similar straining behavior to the elastic stage until macro yielding. Afterwards, the {11.0} grains present a tiny relaxation at about 400 MPa, and the lattice strain curve of {10.0} grains shows an inflection at similar stress, after which the lattice strain is accumulated slower than at the prior stage. Additionally, the {00.2} grains relax when loaded to 420 MPa. The diffraction intensities of variously oriented grains in the peak-aged alloy are quite close to the as-extruded alloy, further confirming the neglect influence of aging treatment on

texture. However, the intensity evolutions of {10.1} and {11.0} grains in the peak-aged alloy are more gradual than those in the as-extruded alloy at the onset of plasticity. It is noteworthy that the evolutions of lattice strains and diffraction intensities in the peak-aged alloy are also correlated with the operation of corresponding slip/twinning mechanisms, as analyzed for the as-extruded alloy in the above.

The above results indicate that peak-aging treatment weakens the stress relaxation in the {10.1} grains. Considering the fact that peak-aging treatment primarily results in the precipitation of β' phases and the concurrent consumption of solute atoms within the Mg matrix, except for which no significant microstructure modifications are observed, it is strongly suggested that the stress relaxation of {10.1} grains is attributed to the interactions between solute atoms and basal dislocations. Cottrell and Bilby [13] firstly proposed that dislocations can attract solute atoms to form atmospheres, as a result of elastic interaction between the two kinds of defects. These solute atmospheres can pin the dislocations. However, when the applied stress is sufficiently high, the dislocations can escape from the atmospheres to be mobile, and the enhancement of mobile dislocation density can lead to the decrease of local stress [20]. Recently, Hu et al. [21] presented a direct evidence for the formation of Cottrell atmospheres around basal dislocations in a Mg-Zn-Y alloy and observed the unpinning of dislocations from the atmospheres. Therefore, it is highly expected that the basal dislocations in the {10.1} grains of

the as-extruded alloy are initially blocked by solute atmospheres. With loading to 360 MPa, the dislocations escape from these atmospheres, resulting in a sudden increase of mobile basal dislocation density. Consequently, the local stress of the {10.1} grains is relaxed abruptly. Furthermore, the massive basal dislocations move instantaneously can cause a sudden change of crystal orientation in the {10.1} grains, giving rise to the corresponding decrease of diffraction intensity of this grain set.

Some previous studies [11, 22] also found the aging treatment can reduce or even eliminate the yield point in Mg alloys. It is likely due to the low number density of precipitates in the aged Mg alloys [1]. Because of this, the amount of dislocations blocked by precipitates is small. Consequently, the increase of mobile dislocation density upon escaping from the precipitates is not significant. Specifically for the present case, the stress relaxation in the peak-aged alloy is also associated with the unpinning of basal dislocations from solute atmospheres survived during the aging treatment, while the initial deviation of the lattice strain curve from elasticity is due to the movement of other basal dislocations which are not pinned by solute atmospheres. Additionally, the significant narrowing of the relaxation extent after peak-aging treatment is attributed to the reduction of the amount of solute atmospheres, resulting from the precipitation of β' phases.

The EVPSC modeling, which focuses on the macro yielding stage, was performed up to the strain of 1.5% for both alloys. In the modeling, the stress relaxation resulting from the unpinning of basal dislocations from solute atmospheres is explicitly taken into account by setting the $\tau_1$ of basal slip in the Voce hardening rule to negative value, representing that basal slip exhibits softening response during the unpinning process. It has been confirmed the LPSO phase with 3% fraction has little effect on the modeling results. Therefore, the LPSO phase is not included in this modeling. The model parameters of both alloys, summarized in Table 1, are obtained by fitting their experimental data. In view of the small imposed strain in the modeling, pyramidal slip is rarely activated, since this slip mode has high CRSS. So the parameters of pyramidal slip weren't identified. Note that the as-extruded alloy has a more negative value of $\tau_1$ and a larger value of $\theta_0$ for basal slip than those in the peak-aged alloy (Table 1), which is due to the sharper and larger stress relaxation in the former alloy than in the latter one (Fig. 4band e).

The comparisons between simulation results and experimental data are presented in Fig. 5. The simulated flow curves have a good match with the experimental ones for both alloys. Furthermore, the model can also well capture the lattice strain evolutions, especially, the stress relaxation of {10.1} grains is well reproduced. The predicted relative mode activities indicate basal and prismatic slips govern the macro yielding in both alloys, which is in good agreement with previous studies [2,23]. Our previous work [24] reveals that, in the bimodal microstructure,

basal slip mainly occurs in the DRXed grains with weak texture, while prismatic slip primarily takes place in the non-DRXed grains with strong <10.0> fiber texture under small strains. Therefore, the parameters of basal slip in Table 1 mainly refer to the DRXed grains, while the parameters of prismatic slip mainly concern the non-DRXed grains. Furthermore, the modeling results validate that the stress relaxation of {10.1} grains in the as-extruded alloy is associated with the sudden increase of the amount of basal dislocations, which is expected to result from the unpinning of basal dislocations from solute atmospheres. The simultaneous activation of massive basal dislocations can cause notable plasticity, thus leading to a rapid decrease of strain hardening rate, namely, an abrupt elastoplastic transition in the as-extruded alloy (Fig. 5a). When the unpinned dislocations encounter solute atoms again or interact with other dislocations, the strain hardening rate will increase. Subsequently, when prismatic slip is notably activated, the hardening rate will decrease again. Therefore, the discontinuous yielding in the as-extruded alloy shown in Fig. 3 is attributed to the interaction between basal dislocations and solute atmospheres. In the peak-aged alloy, however, the interaction between basal dislocations and solute atmospheres is weakened, due to the consumption of a number of solute atoms during aging treatment. Therefore, the activation of basal slip during unpinning process is limited, and prismatic slip need to be significantly activated to accommodate the plasticity, as shown in Fig.

5f. As a consequence, the peak-aged alloy exhibits an extended elastoplastic transition, during which the strain hardening rate is gradually and continuously decreased.

Generally, the yield stress drop and yield plateau in the flow curves are typical features associated with the yield point phenomenon [25]. However, both of these features are not shown in the as-extruded alloy. Instead, the macro stress is continuously increased during the unpinning process. It is primarily due to the deformation inhomogeneity of aggregate resulting from the heterogeneous microstructure. As shown in Fig. 4b, when the {10.1} grains are undergoing stress relaxation, the other grains with harder orientations are bearing more load. Consequently, this composite effect (coexistence of softer and harder grains) makes the macro stress being raised continuously. However, it is expected that this composite effect depends on the recrystallization fraction. With increasing the fraction of DRXed regions, the yield point features will be more obvious.

## 5. Conclusions

The as-extruded Mg-7Gd-2Y-1Zn-0.6Zr (wt. %) alloy exhibits a discontinuous yielding under uniaxial tension along the extrusion direction, which disappears after the peak-aging treatment. The in-situ synchrotron diffraction results indicate the {10.1} grains in the as-extruded alloy exhibit a significant stress relaxation, while in the peak-aged alloy, the relaxation is weakened. It is suggested that the stress relaxation is attributed to the unpinning of basal

dislocations from solute atmospheres. The EVPSC modeling results suggest that the discontinuous yielding in the as-extruded alloy is attributed to the interaction between basal dislocations and solute atmospheres. After peak-aging treatment, the interaction between dislocations and solute atmospheres is weakened due to the consumption of a number of solute atoms, thus resulting in the elimination of discontinuous yielding in the peak-aged alloy.

## Acknowledgements

This research was supported by National Key Research and Development Program of China (No. 2016YFB0301102) and National Natural Science Foundation of China (No. 51571068 and 51771062). The authors thank Prof. Sean R. Agnew in University of Virginia for providing the EVPSC code and thank Prof. Huamiao Wang in Shanghai Jiao Tong University and Dr. Jishnu.J. Bhattacharyya in University of Virginia for providing helpful suggestions on the EVPSC modeling.

Reference

[ 1 ] C. Bettles, M.R. Barnett, (Eds.), 2012. Advances in Wrought Magnesium Alloys: Fundamentals of Processing, Properties and Applications. Elsevier.

[2] S.R. Agnew, D.W. Brown, C.N. Tomé, Validating a polycrystal model for the elastoplastic response of magnesium alloy AZ31 using in situ neutron diffraction, Acta Mater. 54 (2006) 4841-4852.

[3] S.R. Agnew, C.N. Tomé, D.W. Brown, T.M. Holden, S.C. Vogel, Study of slip mechanisms in a magnesium alloy by neutron diffraction and modeling, Scripta Mater. 48 (2003) 1003-1008.

[4] O. Muránsky, M.R. Barnett, D.G. Carr, S.C. Vogel, E.C. Oliver, Investigation of deformation twinning in a fine-grained and coarse-grained ZM20 Mg alloy: Combined in situ neutron diffraction and acoustic emission, Acta Mater. 58 (2010) 1503-1517.

[5] O. Muránsky, M.R. Barnett, V. Luzin, S. Vogel, On the correlation between deformation twinning and Lüders-like deformation in an extruded Mg alloy: In situ neutron diffraction and EPSC. 4 modelling, Mater. Sci. Eng. A 527 (2010) 1383-1394.

[6] S.R. Agnew, R.P. Mulay, F.J. Polesak III, C.A. Calhoun, J.J. Bhattacharyya, B. Clausen, In situ neutron diffraction and polycrystal plasticity modeling of a Mg–Y–Nd–Zr alloy: effects of precipitation on individual deformation mechanisms, Acta Mater. 61 (2013) 3769-3780.

[7] M.R. Barnett, Z. Keshavarz, A.G. Beer, D. Atwell, Influence of grain size on the compressive deformation of wrought Mg–3Al–1Zn, Acta Mater. 52 (2004) 5093-5103.

[8] M.R. Barnett, M.D. Nave, A. Ghaderi, Yield point elongation due to twinning in a magnesium alloy, Acta Mater. 60 (2012) 1433-1443.

[9] J. Zhang, X.F. Zhang, W.G. Li, F.S. Pan, Z.X. Guo, Partition of Er among the constituent phases and the yield phenomenon in a semi-continuously cast Mg–Zn–Zr alloy, Scripta Mater. 63 (2010) 367-370.

[10] N. Stanford, D. Atwell, M.R. Barnett, The effect of Gd on the recrystallisation, texture and deformation behaviour of magnesium-based alloys, Acta Mater. 58 (2010) 6773-6783.

[11] L. Ma, R.K. Mishra, M.P. Balogh, L.M. Peng, A.A. Luo, A.K. Sachdev, W.J. Ding, Effect of Zn on the microstructure evolution of extruded Mg–3Nd (–Zn)–Zr (wt.%) alloys, Mater. Sci. Eng. A 543 (2012) 12-21.

[12] E. Mora, G. Garcés, E. Oñorbe, P. Pérez, P. Adeva, High-strength Mg–Zn–Y alloys produced by powder metallurgy, Scripta Mater. 60 (2009) 776-779.

[13] A.H. Cottrell, B.A. Bilby, Dislocation theory of yielding and strain ageing of iron, Proc. Phys. Soc. London, Sect. A 62 (1949) 49-62.

[14] A. Molinari, G.R. Canova, S. Ahzi, A self consistent approach of the large deformation

polycrystal viscoplasticity, Acta Metall. Mater. 35 (1987) 2983-2994.

[15] H. Wang, P.D. Wu, C.N. Tomé, Y. Huang, A finite strain elastic–viscoplastic self-consistent model for polycrystalline materials, J. Mech. Phys. Solids 58 (2010) 594-612.

[16] R.J. Asaro, A. Needleman, Overview no. 42 Texture development and strain hardening in rate dependent polycrystals, Acta Metall. Mater. 33(1985) 923-953.

[17] T. Homma, N. Kunito, S. Kamado, Fabrication of extraordinary high-strength magnesium alloy by hot extrusion, Scripta Mater. 61 (2009) 644-647.

[18] C. Xu, T. Nakata, X.G. Qiao, M.Y. Zheng, K. Wu, S. Kamado, Ageing behavior of extruded Mg–8.2Gd–3.8Y–1.0Zn–0.4Zr (wt.%) alloy containing LPSO phase and γ′ precipitates, Sci. Rep. 7, 40846; doi: 10.1038/srep40846 (2017).

[19] D.W. Brown, S.R. Agnew, M.A.M. Bourke, T.M. Holden, S.C. Vogel, C.N. Tomé, Internal strain and texture evolution during deformation twinning in magnesium, Mater. Sci. Eng. A 399 (2005) 1-12.

[20] G.T. Hahn, A model for yielding with special reference to the yield-point phenomena of iron and related bcc metals, Acta Metall. 10 (1962) 727-738.

[21] W.W. Hu, Z.Q. Yang, H.Q. Ye, Cottrell atmospheres along dislocations in long-period stacking ordered phases in a Mg–Zn–Y alloy, Scripta Mater. 117 (2016) 77-80.

[22] W. Rong, Y. Zhang, Y.J. Wu, M. Sun, J. Chen, Y. Wang, J.Y. Han, L.M. Peng, H.X. Ding, Effects of Zr and Mn additions on formation of LPSO structure and dynamic recrystallization behavior of Mg-15Gd-1Zn alloy, J. Alloys Compd. 692 (2017) 805-816.

[23] H. Wang, P.D. Wu, C.N. Tomé, J. Wang, Study of lattice strains in magnesium alloy AZ31 based on a large strain elastic-viscoplastic self-consistent polycrystal model, Int. J. Solids Struct. 49 (2012) 2155-2167.

[24] C. Xu, G.H. Fan, T. Nakata, X. Liang, Y.Q. Chi, X.G. Qiao, G.J. Cao, T.T. Zhang, M. Huang, K.S. Miao, M.Y. Zheng, S. Kamado, H.L. Xie, Deformation Behavior of Ultra-Strong and Ductile Mg-Gd-Y-Zn-Zr Alloy with Bimodal Microstructure, Metall. Mater. Trans. A 49 (2018) 1931-1947.

[25] E.O. Hall, Yield point phenomena in metals and alloys, Macmillan, 1970.

Figure(s)

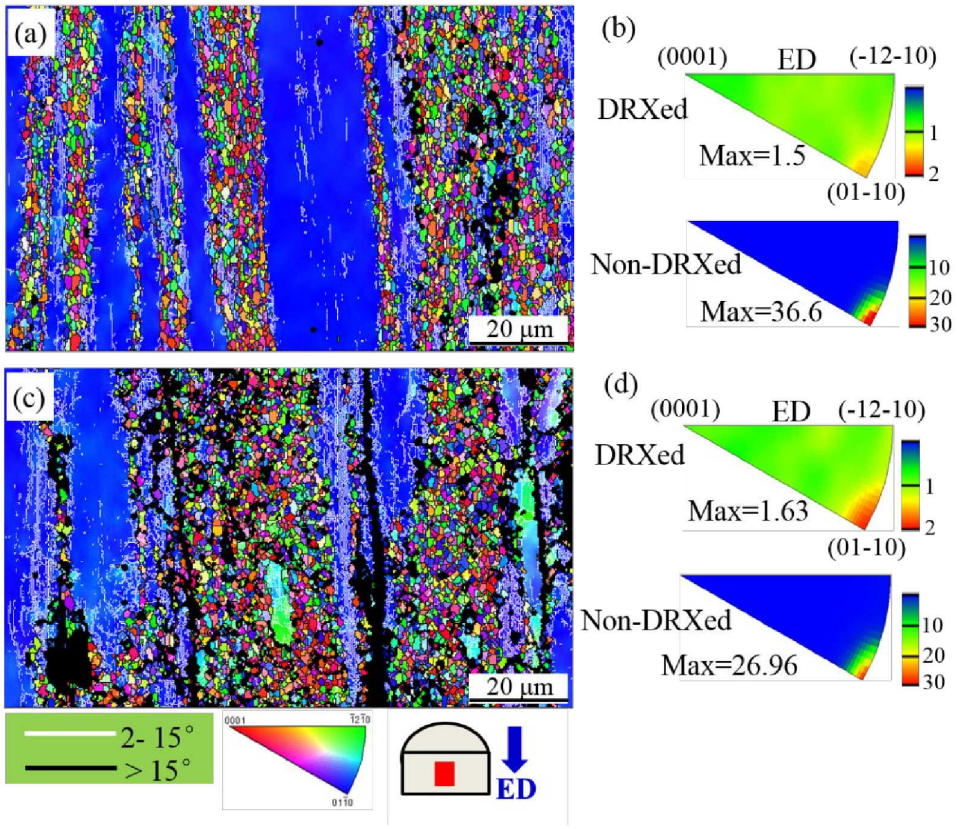


Fig. 1 EBSD results of the as-extruded and peak-aged alloys: (a),(b) as-extruded alloy; (c),(d) peak-aged alloy; (a),(c) IPF maps; (b),(d) inverse pole figures with respect to ED.

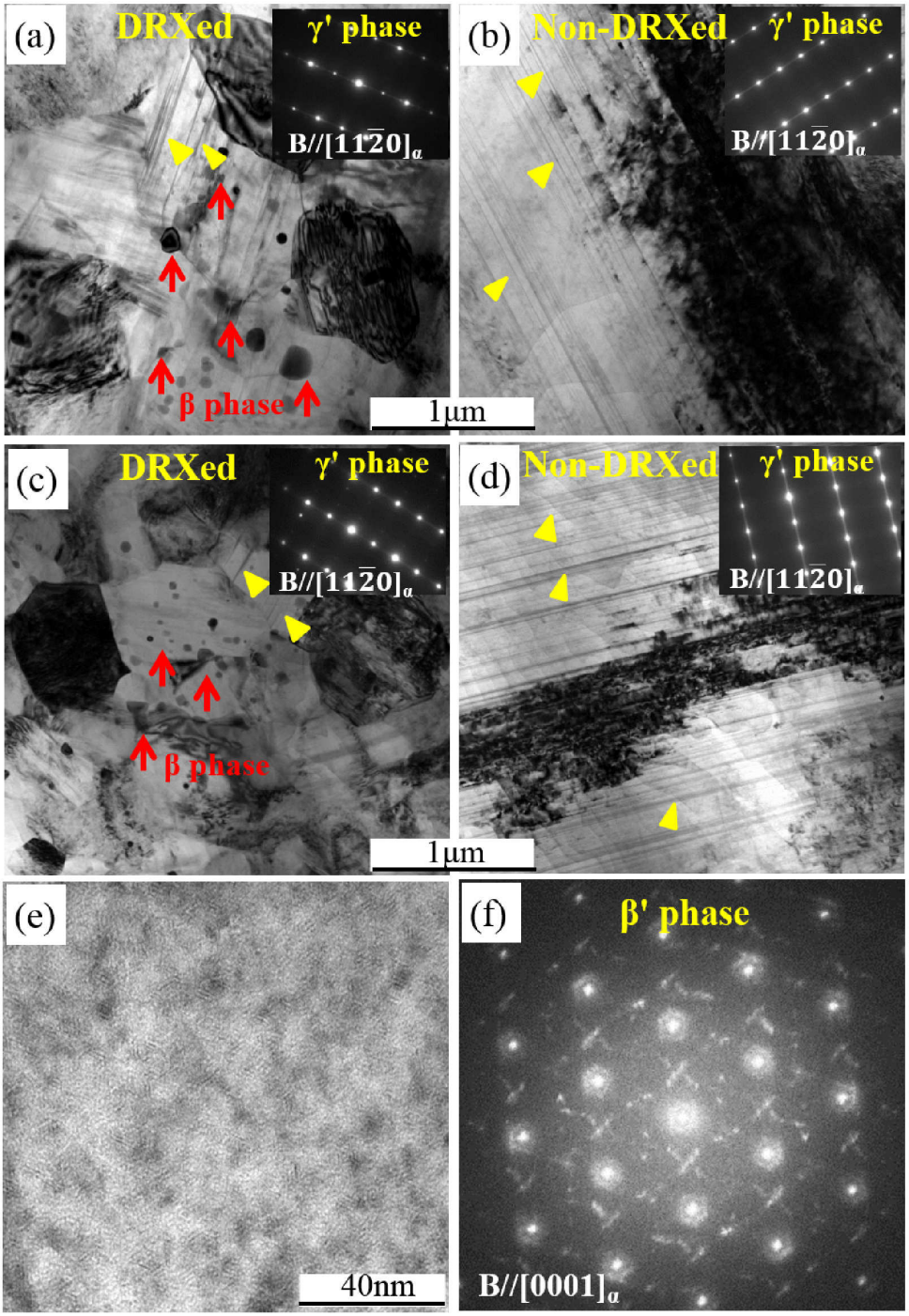


Fig. 2 TEM micrographs of the as-extruded and peak-aged alloys: (a)-(b) as-extruded alloy; (c)-(f) peak-aged alloy; (f) the selected area electron diffraction (SAED) pattern of (e). The inserts in Fig. 2a-d show the SAED patterns of the lamellar phases indicated by the triangles in respective micrographs.

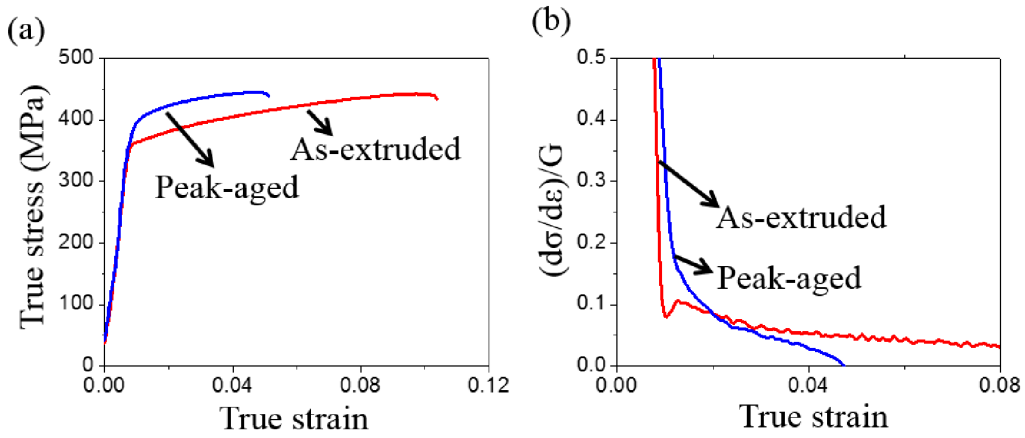


Fig. 3 (a) Tensile flow curves of the as-extruded and peak-aged alloys; (b) Strain hardening rates calculated from (a), normalized by the shear modules of Mg.

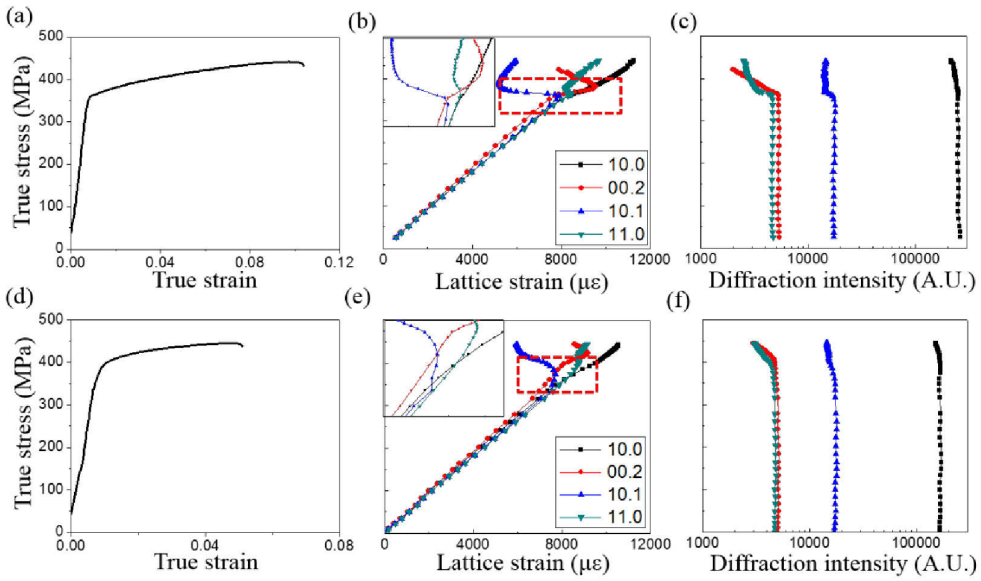


Fig. 4 The flow curves, lattice strains and diffraction intensities of the as-extruded and peak-aged alloys plotted as functions of the applied macroscopic stress: (a)-(c) as-extruded alloy; (d)-(f) peak-aged alloy. The inserts in (b) and (e) are enlarged graphs of the regions marked by rectangles in (b) and (e), respectively.

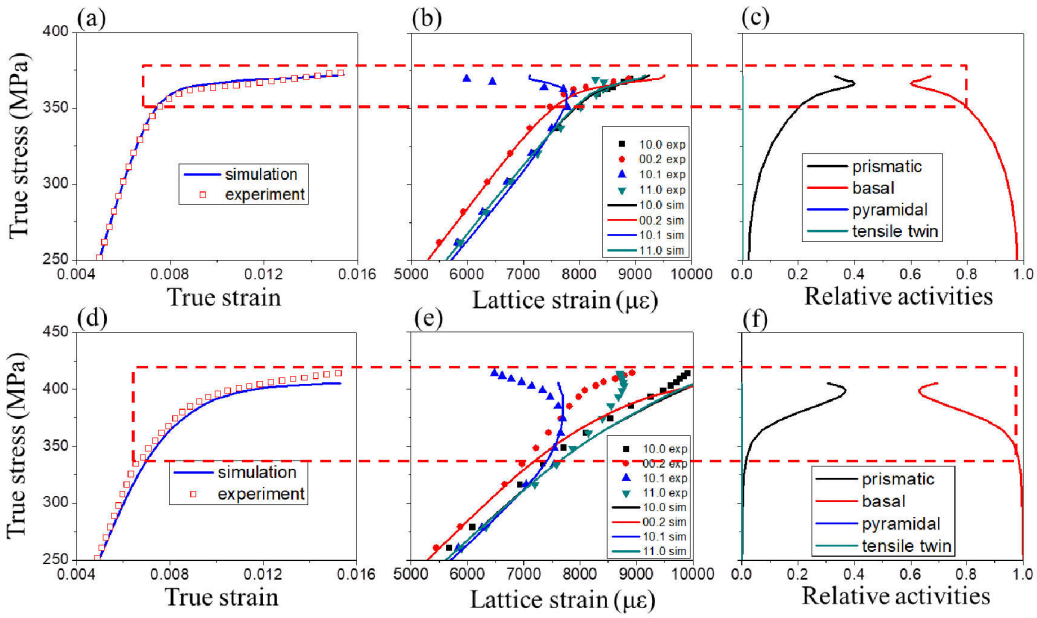


Fig. 5 Comparisons between EVPSC modeling results and experimental data, including flow curves, lattice strain evolutions and predicted relative mode activities: (a)-(c) as-extruded alloy; (d)-(f) peak-aged alloy. The elastoplastic transition in both alloys is marked by rectangle.

**Table(s)**

Table 1 EVPSC model parameters (MPa) for the as-extruded and peak-aged alloys.

| Alloy | Mode | $\tau_0$ | $\tau_1$ | $\theta_0$ | $\theta_1$ |
|---|---|---|---|---|---|
| As-extruded | Basal | 128 | -90 | 10000 | 0 |
| | Prismatic | 167 | 100 | 1000 | 0 |
| | Pyramidal | - | - | - | - |
| | Tensile twin | 300 | 0 | 0 | 0 |
| Peak-aged | Basal | 120 | -85 | 7500 | 0 |
| | Prismatic | 190 | 100 | 1000 | 0 |
| | pyramidal | - | - | - | - |
| | Tensile twin | 350 | 0 | 0 | 0 |